

Running Gluon Mass from Landau Gauge Lattice QCD Propagator

O. Oliveira

Departamento de Física, Universidade de Coimbra, 3004-516 Coimbra, Portugal

Departamento de Física, Instituto Tecnológico de Aeronáutica, 12.228-900 São José dos Campos, SP, Brazil

E-mail: orlando@teor.fis.uc.pt

P. Bicudo

Departamento de Física, I.S.T., Av Rovisco Pais, 1049-001 Lisboa, Portugal

E-mail: bicudo@ist.utl.pt

Abstract. The interpretation of the Landau gauge lattice gluon propagator as a massive type bosonic propagator is investigated. Three different scenarios are discussed: i) an infrared constant gluon mass; ii) an ultraviolet constant gluon mass; iii) a momentum dependent mass. We find that the infrared data can be associated with a massive propagator up to momenta ~ 500 MeV, with a constant gluon mass of 723(11) MeV, if one excludes the zero momentum gluon propagator from the analysis, or 648(7) MeV, if the zero momentum gluon propagator is included in the data sets. The ultraviolet lattice data is not compatible with a massive type propagator with a constant mass. The scenario of a momentum dependent gluon mass gives a decreasing mass with the momentum, which vanishes in the deep ultraviolet region. Furthermore, we show that the functional forms used to describe the decoupling like solution of the Dyson-Schwinger equations are compatible with the lattice data with similar mass scales.

PACS numbers: 14.70.Dj; 11.15.Ha; 12.38.-t

1. Introduction and Motivation

The lagrangian for pure SU(3) Yang-Mills theory does not include a mass scale. At the classical level, conformal invariance of pure gauge theories is the expression of this lack of scale. However, the corresponding quantum theory gets a mass, let us say Λ_{QCD} , from the loop contributions via dimensional transmutation.

At the level of the lagrangian a gluon mass term is forbidden by gauge invariance and, as long as the color symmetry is unbroken, the gluon is supposed to be massless. Certainly, in what concerns the perturbative solution of QCD, within the framework of the Faddeev-Popov quantization procedure [1], the gluon is massless. However, as discussed in [2], a dynamical generated mass which is a function of the momentum is allowed if one goes beyond perturbation theory.

From the theoretical point of view, a non-vanishing gluon mass is welcome to regularize infrared divergences and to solve some problems related with unitarity. On the other side, diffractive phenomena [3] and inclusive radiative decays of J/ψ and Υ [4] suggest a massive gluon. Moreover, lattice simulations suggest an infrared gluon hard mass of ~ 600 MeV [5] and an ultraviolet mass $M_g \sim 1.0$ GeV [19, 20]. Phenomenology favors a gluon mass between ~ 0.500 GeV and ~ 1.2 GeV depending on how the mass is defined – see table 15 in [4]. Furthermore, a dynamically generated gluon mass can be related with the presence of the $\langle A^2 \rangle$ gluon condensate, which is associated with the non-perturbative sector of QCD and whose role has been investigated by several authors - see, for example, [6, 7, 8] and references therein.

The idea of a gluon mass was explored by different authors [9, 10, 11, 12, 13, 14, 15, 16]. Starting from the Dyson-Schwinger equations (DSE) for the gluon and ghost propagators, after a suitable truncation scheme, the equations were solved and the transverse part of the gluon propagator described by a massive type propagator, i.e.

$$D(q^2) = \frac{Z(q^2)}{q^2 + M^2(q^2)}, \quad (1)$$

with a momentum dependent gluon mass $M^2(q^2)$, called below running mass gluon, and a running dressing function $Z(q^2)$. Typically, the numerical solution for the propagator is fitted to a functional form $M^2(q^2)$ copied from the solution discussed in [2]. The solutions of the DSE give a $M(q^2)$ which takes its largest value at zero momentum, where $M(0) \sim 600$ MeV, and vanishes for $q \gg \Lambda_{QCD}$. In this way, the usual perturbative propagator is recovered at high momentum.

The Dyson-Schwinger studies referred to in the above paragraph rely on the Faddeev-Popov quantization method, whose validity for investigating non-perturbative effects in QCD is under debate - see, for example, [17, 18] and references therein. However, a running gluon mass was also found within the studies of the non-perturbative quantization of Yang-Mills theories. In particular, in the framework of the so-called refined Gribov-Zwanziger action [18], a tree level propagator was computed suggesting a functional form for $M(q^2)$ which is close to the original proposal of Cornwall [2].

Besides the solutions of the Dyson-Schwinger equations, lattice simulations also

provide support for a non-vanishing gluon mass, see for example [5, 19, 20, 21]. The precise value for $M(q^2)$ depends on how the gluon propagator is modeled. For example, in lattice QCD or Dyson-Schwinger calculations, a running mass is computed fitting the propagator to a given functional form for $M(q^2)$. In this work we use lattice QCD simulations to investigate $M^2(q^2)$. Besides checking the compatibility of the lattice data with theoretical predictions for $M^2(q^2)$, a first attempt is made to compute the running gluon mass directly from lattice simulations.

The paper is organized as follows. In section 2 we describe the lattice setup, the cuts performed to produce a unique curve for the gluon propagator and the renormalization procedure. The gluon mass is investigated in section 3 considering three different scenarios. Before considering the running mass, we consider constant mass ansatzes to fit the propagator for the infrared (section 3.1.1) and the ultraviolet momenta (section 3.1.2). We find that the gluon propagator cannot be fully fitted with a constant gluon mass, and thus we proceed with fitting the gluon propagator with a running mass gluon and a running gluon dressing function (3.2). Finally, in section 4 we resume the results of section 3 and comment on its interpretation.

2. Definitions and Lattice Setup

In this paper we consider four dimensional SU(3) Wilson action lattice simulations at $\beta = 6.0$. For this β value the lattice spacing, measured from the string tension [22], is given by $a = 0.1016(25)$ fm or, equivalently, $a^{-1} = 1.943$ GeV.

The gauge configurations were generated with the MILC code [23]. Each configuration, sampled with the Wilson action, was rotated to the Landau gauge, as described in [20], using for gauge fixing the overrelaxation algorithm. The gauge fixing process requires a maximization of a given functional over the gauge orbit of each configuration. The maximization process was stopped when the lattice tetra-divergence [20], averaged per site, become smaller than 10^{-13} . The set of lattices considered in the present work are summarized in table 1.

In the Landau gauge, the gluon propagator is given by

$$D_{\mu\nu}^{ab}(q^2) = \langle A_\mu^a(q) A_\nu^b \rangle = \delta^{ab} \left(\delta_{\mu\nu} - \frac{q_\mu q_\nu}{q^2} \right) D(q^2); \quad (2)$$

latin letters stand for color indices and greek letters for space-time indices. The momentum space gluon field $A_\mu^a(q)$ definition and how to compute the form factor $D(q^2)$ are described in [20] and will not be repeated here.

For the continuum momentum we take the standard definition

$$q_\mu = \frac{2}{a} \sin \left(\frac{\pi}{L_\mu} n \right), \quad n = 0, \dots, L_\mu - 1, \quad (3)$$

where a is the lattice spacing and L_μ the number of lattice points in direction μ .

In the following only renormalized data will be considered. The renormalization was performed fitting, for each lattice simulation, the bare lattice propagator to the

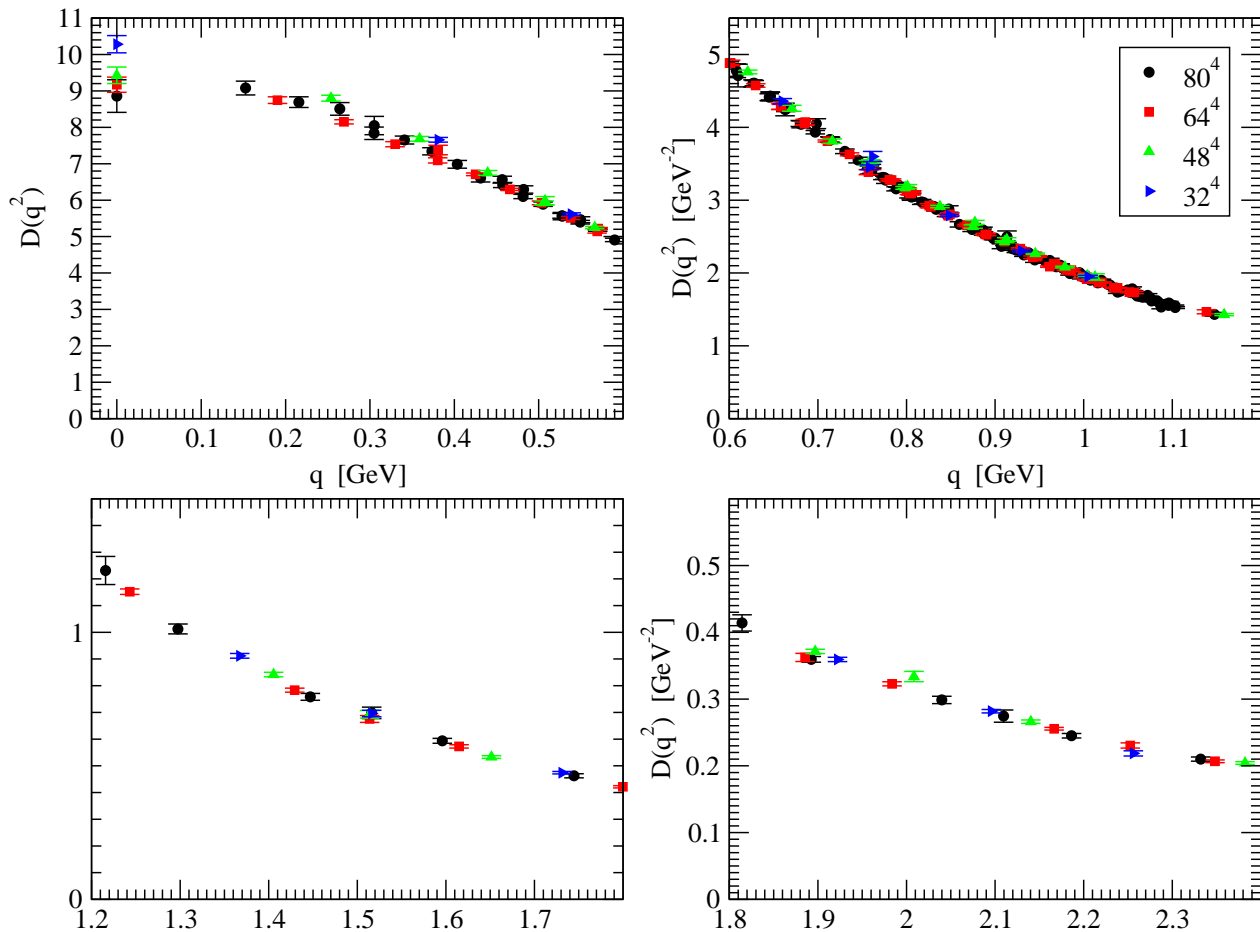


Figure 1. Renormalized gluon propagator for all the lattices described in table 1. The propagator (vertical axis) is given in GeV^{-2} and the momenta (horizontal axis) in GeV .

one-loop inspired result

$$D(q^2) = \frac{K}{q^2} \left(\ln \frac{q^2}{\Lambda^2} \right)^{-\gamma}, \quad (4)$$

where $\gamma = 13/22$ is the gluon anomalous dimension. For the fits to equation (4), the largest momentum range, starting at q_{min} and going up to $\sim 5 \text{ GeV}$, with the $\chi^2/d.of.$ closer to unity was used – see table 2. From the fits we extracted the constants K and Λ , which enabled the computation of the renormalization constant Z_R via

$$D(q^2) = Z_R D_{Lat}(q^2), \quad (5)$$

after requiring the renormalized propagator to be given by

$$D(q^2)|_{q^2=\mu^2} = \frac{1}{\mu^2}. \quad (6)$$

As renormalization scale it was used $\mu = 3 \text{ GeV}$.

All the simulations were performed on an hypercubic lattice which breaks rotational invariance. In order to reduce lattice spacing effects, for each lattice and for momenta

L	32	48	64	80
L(fm)	3.2	4.9	6.5	8.1
# Confs.	126	104	120	50

Table 1. Lattice setup - the lattices considered are L^4 symmetric hypercubes. For conversion into physical units the lattice spacing we used $a = 0.1016(25)$ fm, or $a^{-1} = 1.943$ GeV, as computed from the string tension [22].

L	32	48	64	80
$q_{min} - q_{max}$ (GeV)	2.81 - 5.08	2.49 - 5.02	1.51 - 5.14	1.52 - 5.05
$\chi^2/d.o.f.$	0.91	0.97	0.89	1.06
Z_R (GeV $^{-2}$)	0.149(21)	0.149(18)	0.1477(38)	0.1478(53)

Table 2. Fits of the conic cut propagator data to equation (4) and renormalization constants as function of the the lattice volume. q_{min} and q_{max} stand for the lowest and highest momenta, respectively, used in the fit to get Z_R .

$q > 1$ GeV the conic cut [19] was applied. For momenta below 1 GeV, all the data points were considered. In this way, we hope to have a good description of the infrared region. The renormalization procedure, as described above, was performed separately for each lattice propagator. In all cases the fit to equation (4) was smooth and the corresponding $\chi^2/d.o.f. \sim 1$. The renormalized gluon propagator, after the cuts just described, is reported in figure 1. As can be seen in figure 1, finite volume effects are observed in our data.

In the following, we will consider two different analysis of the lattice data: (i) a separate analysis for each lattice volume; (ii) the different lattices can be combined, after removing finite volume effects, to produce a propagator with a larger density of points in the momenta axis. If the different volumes allow for an evaluation of the finite volume effects, the combined data, with its larger density of points on the q -axis, will reduce the statistical error on the final result.

Let us elaborate more on the combined data set. From figure 1 it is clear that the lattice propagator differ by more than one standard deviation as a function of the physical volume. This effect is clearly seen in the infrared region. To reduce the finite volume effects, we take the propagator from the largest volume considered here, corresponding to an 80^4 lattice, as a reference and compare all the remain propagators to it. To reduce the finite volume effects, the infrared data of the smaller lattices was removed if the propagator was not compatible, within one standard deviation, with the 80^4 propagator. Due to the infrared cut, from the 64^4 propagator only data with $q \geq 425$ MeV was considered, from 48^4 only $q \geq 671$ MeV data was considered and from 32^4 only data with $q \geq 848$ MeV was included.

The cuts just described do not remove all lattice spacing effects. Indeed, even after performing all the cuts one can observe data points where, for the same q^2 the propagator differ by more than one standard deviation. The difference is due to the

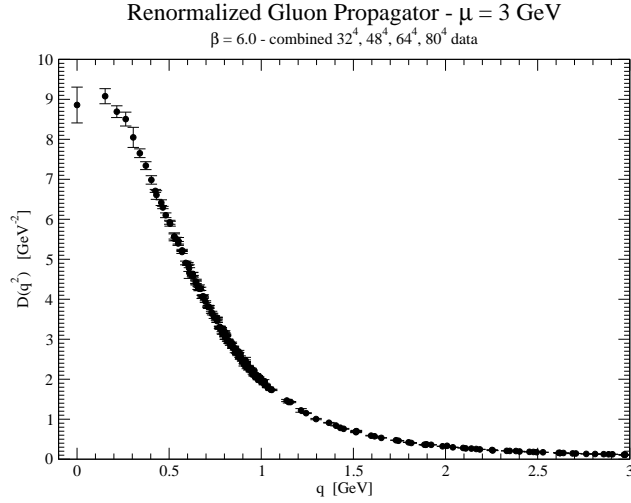


Figure 2. Renormalized gluon propagator $D(q^2)$.

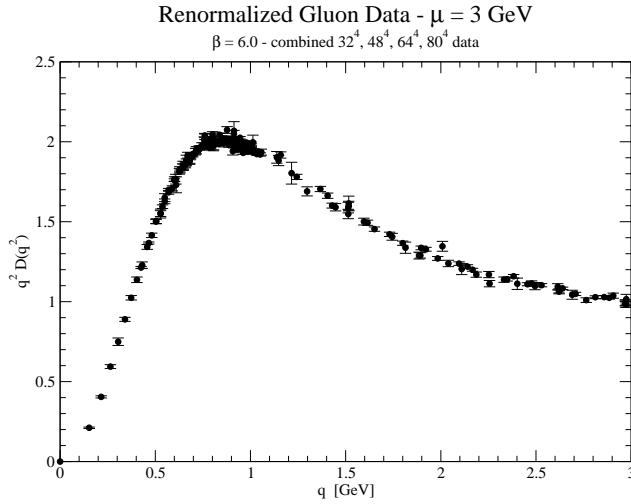


Figure 3. Renormalized gluon data for $q^2 D(q^2)$.

violation of rotational invariance. Therefore, to minimize such type of effects, for each lattice volume and for the same q^2 coming from different q_μ , if the different estimates of the propagator don't agree within one standard deviation, one of the points is excluded. For example, for the 80^4 lattice for momentum $q = 457$ MeV there are two estimates for the gluon propagator, $D(q^2) = 6.563(95)$ GeV^{-2} associated with the lattice direction $n = (3, 0, 0, 0)$ and $D(q^2) = 6.416(71)$ GeV^{-2} associated with the lattice direction $n = (2, 2, 1, 0)$, coming from different types of momenta. The first value is clearly above all the data points and it was not considered in the data sets. In this way, the surviving points will produce a unique curve for $D(q^2)$.

The combined lattice data for gluon propagator, after performing all the cuts, is shown in figure 2. The corresponding $q^2 D(q^2)$ function is reported in figure 3. Figures 2 and 3 suggest that both finite volume and finite lattice spacings have been removed from our data.

The largest lattice volume included in our simulation is $(8.1 \text{ fm})^4$. Lattice gluon propagators computed with larger volumes, but with a lattice spacing about twice the spacing considered in the present work, were reported in [24]. The two sets of data were compared in [8]. We will not repeat this exercise but will resume the outcome of the comparison. The propagator used in this work and those of [24] are essentially the same. Indeed, they are compatible within one standard deviation for $q > 200 \text{ MeV}$ and show a small difference for smaller momenta. For $q < 200 \text{ MeV}$ the propagator of [24] is about 10% smaller than the data in figure 2. As seen in figure 1, our simulations have a limited access to momenta below 200 MeV and, in this way, we expect that the impact of the finite volume effects on $M^2(q^2)$ computed from the combined data set is well below 10% factor. Furthermore, the separate analysis of the each volume will provide an estimate of the finite volume effects on the running mass.

Another source of systematics are Gribov copies, i.e. configurations which satisfy the Landau gauge condition but are related by finite gauge transformations. This is a difficult and computational very demanding problem for the lattice practitioner. However, the known SU(3) lattice simulations show that Gribov copies do not change significantly the gluon propagator, i.e. that the effect due to the copies are, typically, within the statistical error; see, for example, [20]. Therefore, in this work we will ignore possible effects due to the Gribov copies.

3. The Gluon Mass

Our goal is to obtain the gluon mass M . However, its computation, or the calculation of M^2 , is not independent of the estimation of the dressing function Z . In the next sections we look at the gluon mass as given by the gluon propagator, i.e. by equation (1), and explore different definitions. First we consider constant mass ansatze to fit the propagator for the infrared and the ultraviolet momenta. However, the gluon propagator cannot be fitted over all momenta with a constant gluon mass. Then, we proceed fitting the gluon propagator with a momentum dependent mass, called below running mass gluon, and a running gluon dressing function.

3.1. Constant Gluon Mass

We start our analysis assuming a constant gluon mass, i.e. assuming that in equation (1) M and Z are constants. Therefore, in this section we take the gluon propagator as being described by

$$D(q^2) = \frac{Z}{q^2 + M^2} \tag{7}$$

in a certain momentum range.

3.1.1. Fitting of a Constant Infrared Gluon Mass To check if the infrared gluon propagator can be described by such type of model, the lattice data was fitted to

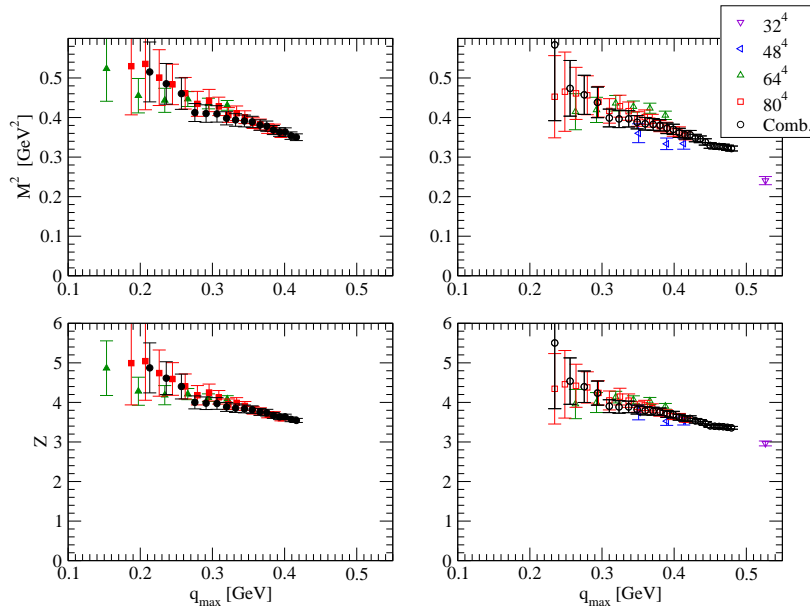


Figure 4. Results of fitting the infrared lattice propagators to equation (7) in the range $[0, q_{max}]$ and for $\chi^2/d.o.f. \leq 2.0$. In figure full symbols refers to fits including the zero momentum propagator, while open symbols mean that $D(0)$ was removed from the data sets.

equation (7) in the momentum range $[0, q_{max}]$. The results are plotted in figure 4, where full symbols mean that the zero momentum propagator was included in the fits, while open symbols mean that $D(0)$ was removed from the data sets.

Figure 4 shows a M^2 and Z that are, within one standard deviation, independent of the fitting range, i.e. of q_{max} . Furthermore, requiring a $\chi^2/d.o.f. < 2.0$ means that the infrared propagator can be described by (7) for momenta up to $q \sim 500$ MeV, if one ignores the lattice estimate for $D(0)$, and up to $q \sim 430$ MeV, if the lattice $D(0)$ is included in the data set. More, only for volumes of $\sim (6.5 \text{ fm})^4$ or larger, the infrared lattice propagator can be described by a massive type propagator if $D(0)$ is taken into account in the data sets.

Values for Z , M and q_{max} for each data set are reported in table 3. The table includes only the results of the fits whose $\chi^2/d.o.f.$ is closer to unit. If one includes $D(0)$ in the data, Z and M seem to be essentially independent of the volume. However, if one removes the zero momentum propagator from the data set, then one can observe a slightly volume dependence with M and Z increasing with V . In both cases discussed, i.e. including or not $D(0)$, M and Z computed from the combined data is just below the corresponding values obtained from the two largest two volumes.

For the fits where $D(0)$ is excluded, a linear extrapolation of M and Z with $1/L$ towards the infinite volume can be performed. Only after disregarding the 64^4 results one is able to obtain excellent extrapolations. Note that the numbers reported for the fits to the 64^4 lattice propagator are off the main trend observed in the remaining fits. The linear extrapolation to the infinite volume give $Z = 4.49(10)$ with $\chi^2/d.o.f. = 0.38$

L	32	48	64	80	Comb.
Including $D(0)$					
q_{max} (MeV)	–	–	503	482	528
Z	–	–	4.082(86)	3.99(13)	3.760(87)
M (MeV)	–	–	656(10)	641(10)	617(11)
$\chi^2/d.o.f.$	–	–	0.74	1.15	1.14
Excluding $D(0)$					
q_{max} (MeV)	660	508	503	505	550
Z	2.963(62)	3.53(10)	4.035(89)	3.85(11)	3.594(68)
M (MeV)	490(11)	578(12)	651(10)	626(13)	597(9)
$\chi^2/d.o.f.$	1.42	0.99	0.39	0.95	1.03

Table 3. Results of fitting equation (7). The values of M and Z reported are for the fits whose $\chi^2/d.o.f.$ is closer to unit for each data set.

and $M = 723(11)$ MeV for a $\chi^2/d.o.f. = 0.70$. To these extrapolated values corresponds a

$$D(0)_{V=\infty} = 8.58(26) \quad \text{GeV}^{-2}, \quad (8)$$

in excellent agreement with the largest volume simulated here, $D(0)_{V=(8.1 \text{ fm})^4} = 8.86(45) \text{ GeV}^{-2}$, and with the infinite volume extrapolation computed in [8], $D(0) = 8.3(5) \text{ GeV}^{-2}$. Further, the value (8) agrees with the $D(0)$ computed using large volumes and reported in [8].

Our conclusion being that the fits show that the infrared lattice propagator is well described by a massive type propagator from momenta up to ~ 500 MeV with an effective gluon mass around $650 - 700$ MeV. From table 3, it follows that if $D(0)$ is included in the data set, then a massive type propagator describes the lattice data up to moment ~ 500 MeV with $Z = 4.044(78)$ and $M = 648(7)$ MeV given by the average values of the 64^4 and 80^4 figures; errors computed assuming gaussian error propagation. On the other hand, if one excludes $D(0)$ from the data sets, again a massive type propagator describes well the infrared lattice data up to $q \sim 500$ MeV with $Z = 4.49(10)$ and an effective gluon mass $M = 723(11)$ MeV.

3.1.2. Fitting a Constant Ultraviolet Gluon Mass The same reasoning applied to infrared can be used to investigate the high momenta region. However, for the high momenta the fits to (7) give a negative M^2 , with M^2 depending strongly on the fitting range. We take this result as an indication that the ultraviolet is not described by such a propagator.

Our discussion of the high momentum region is not in contradiction with the results of [19, 20], where an ultraviolet gluon mass of ~ 1 GeV was claimed. In [19, 20] an

ultraviolet regulator was used and the lattice data surviving the conic cut fitted to

$$D(q^2) = Z \frac{\left[\frac{1}{2} \ln(q^2 + M^2)(q^{-2} + M^{-2}) \right]^{-\gamma}}{q^2 + M^2}, \quad (9)$$

where M is the gluon mass. Notice that the positive gluon mass in the numerator of eq. (9) is equivalent to a negative mass in the denominator of eq. (7), and thus a negative ultraviolet mass, in the sense of eq. (7), is not in contradistinction with perturbative QCD.

3.2. Momentum Dependent Gluon Mass

The lattice gluon propagator can be described by a massive type propagator in the infrared region. For ultraviolet momenta, the propagator follows closely the 1-loop perturbative prediction and, in this sense, one can claim that for the high momenta region the effective gluon mass vanishes. Therefore, a way of recovering this two results is through the introduction of an effective gluon mass which is a function of the gluon momenta. So let us assume that $D(q^2)$ is given by equation (1) and that $M(q^2)$ and the dressing function $Z(q^2)$ that are functions of the momentum. In the following we will refer to $M(q^2)$ and $Z(q^2)$ as the running mass and running dressing function, respectively.

Our first try to compute $M(q^2)$ and $Z(q^2)$ is to reproduce the analysis of the two previous sections. After dividing the q -axis into small window momenta and, in each momenta window, fit the propagator assuming Z and M constant, the outcome is a decreasing $M^2(q^2)$ with q^2 and, for momenta above ~ 1 GeV, $M^2(q^2)$ becomes negative. Given that the computation of Z and M^2 are not independent, a negative mass squared is, certainly, due to a will conditioning of at least one of the functions. Further, the problem of a negative mass squared can be cured, for example, by changing the definition of Z . This requires some model building and, instead, we will proceed fitting the lattice data to well known functional formulas.

Although, the outcome of this procedure to compute $M^2(q^2)$ and $Z(q^2)$ will not be reported here, we would like to call the reader attention to some results found when analyzed the running mass and dressing functions obtained as described in the previous paragraph.

In what concerns $M^2(q^2)$, we find that in the infrared region it agrees well with the results reported in section 3.1.1. Further, $M^2(q^2)$ follows a q^2 behavior in the infrared region and the lattice data can be fitted assuming $M^2(q^2) \sim q^2 \ln q^2$ as suggest in [2].

The running gluon dressing function $Z(q^2)$ decreases linearly from $q = 0$ up to 1 GeV. In the ultraviolet region, $Z(q^2)$ agrees well with the perturbative QCD prediction. We observed that the gluon dressing function is well described by the functional formula

$$Z(q^2) = \frac{Z_0}{[A + \ln(q^2 + m_0^2)]^\gamma}, \quad (10)$$

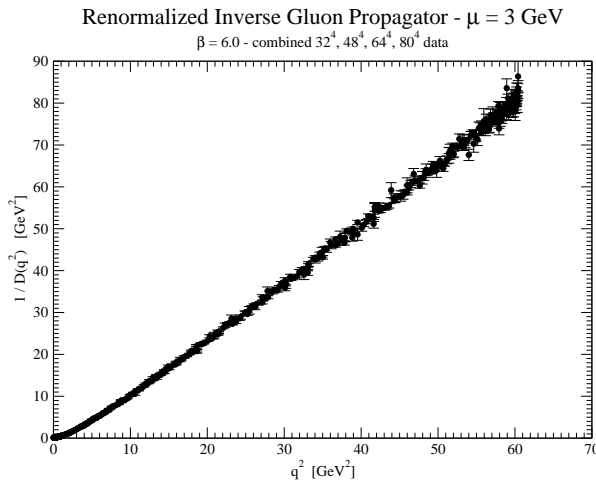


Figure 5. Inverse gluon propagator for the combined data set. Note the "almost" linear behaviour with q^2 of $1/D(q^2)$.

where $\gamma = 13/22$ is the anomalous gluon dimension and $m_0^2 \sim 1.6 \text{ GeV}^2$. Note that in equation (10), m_0^2 plays a role similar to M^2 in (9). In [19, 20], the authors measured a $M = 1.0(1) \text{ GeV}$. The fits give essentially the same value, i.e. an $m_0 \sim 1.3 \text{ GeV}$.

In figure 5 the inverse of the propagator is plotted, for the combined data set, against q^2 . The figure shows that $1/D(q^2)$ follows essentially the perturbative behavior at large momenta, i.e. $1/D(q^2) \propto q^2$, and at smaller momenta the data points deviate from a pure quadratic behavior. Not surprisingly, the observed ultraviolet confirms that $D(q^2)$ is well described by equation (4).

3.2.1. $M^2(q^2)$ from a Perturbative Inspired $Z(q^2)$: An effective gluon mass can be defined extending the perturbative behavior, observed in the high momentum region, towards the infrared region. Indeed, if one assumes that

$$Z(q^2) = z \left[\log \left(1 + \frac{q^2}{\Lambda^2} \right) \right]^{-\gamma} \quad (11)$$

is valid over all momentum range, which ensures that the gluon dressing function is finite everywhere, z and Λ can be measured fitting the ultraviolet lattice gluon data to

$$D(q^2) = \frac{z \left[\log \left(1 + \frac{q^2}{\Lambda^2} \right) \right]^{-\gamma}}{q^2}, \quad (12)$$

in a given range of momenta $[q_{min}, q_{max}]$. The running gluon mass is then defined by taking the lattice propagator as

$$D(q^2) = \frac{z \left[\log \left(1 + \frac{q^2}{\Lambda^2} \right) \right]^{-\gamma}}{q^2 + M^2(q^2)} \quad (13)$$

for all q . With this definition, called below $M_{pert}(q^2)$, one ensures that the usual perturbative propagator is recovered for high momenta or, equivalently, that $M_{pert}(q^2) \rightarrow 0$ for sufficiently high q . As described below, the gluon becomes massless

L	q_{min} (GeV)	z	Λ (GeV)	$\chi^2/d.o.f.$	# d.of.
32	3	1.852(68)	0.726(79)	0.96	11
	3.5	1.78(11)	0.83(14)	1.11	9
	4	1.54(20)	1.22(39)	1.00	6
48	3	1.830(75)	0.774(92)	1.21	15
	3.5	2.00(12)	0.58(12)	0.78	11
	4	2.16(29)	0.43(23)	1.01	8
64	3	1.728(51)	0.879(71)	1.10	20
	3.5	1.886(88)	0.67(10)	0.78	15
	4	1.89(19)	0.66(22)	0.98	11
80	3	1.761(86)	0.83(11)	1.27	25
	3.5	2.05(18)	0.50(16)	1.04	19
	4	2.04(28)	0.51(26)	0.96	14
Comb	3	1.783(37)	0.812(47)	1.33	68
	3.5	1.904(63)	0.661(72)	1.13	54
	4	1.92(12)	0.64(14)	1.16	39

Table 4. Results of fitting equation (12) for $q \in [q_{min}, q_{max}]$ for $q_{max} = 5$ GeV.

for $q \sim 1$ GeV, which a surprisingly low mass scale. Of course, the exact momentum scale at which the gluon becomes massless is connected with the parameterization of the gluon dressing function $Z(q^2)$.

The results of fitting the lattice data to equation (12), for $q \in [q_{min}, q_{max}]$ and $q_{max} = 5$ GeV, are summarized in table 4. The reason to exclude momenta above 5 GeV is to avoid remaining lattice artifacts which were not removed by the renormalization procedure. In what concerns q_{min} , it should belong to a region where the perturbative behavior is recovered. The renormalization procedure described previously, see section 2 and table 2, suggests that $q_{min} = 3$ GeV belongs already to the perturbative region. The two remaining q_{min} values, i.e. 3.5 GeV and 4 GeV, were used to check for the stability of the fits.

The results reported in table 4 show that, for all the data sets, equation (12) describes well the lattice propagators in all momenta windows considered. Further, within each data set, z and Λ computed for the different q_{min} are compatible within one standard deviation. There are a few exceptions, where the z and/or Λ become compatible with the figures of the fits having the larger number of *d.o.f.* within less than two standard deviations, namely the fits to the 32^4 data with the smallest momentum range, the Λ from fits to the 48^4 propagator with the smallest momentum range, the fits to 64^4 data with $q_{min} = 3.5$ GeV, the Λ from fits to the 80^4 propagator with $q_{min} = 3.5$ GeV, the fits to the combined data set with $q_{min} = 3.5$ GeV. Moreover, comparing the fits with the larger number of degrees of freedom, it follows that z and Λ , for all data sets are, compatible within one standard deviation. Given the good stability of the fits, in the following, we will use the results from the fits with the largest number of degrees of

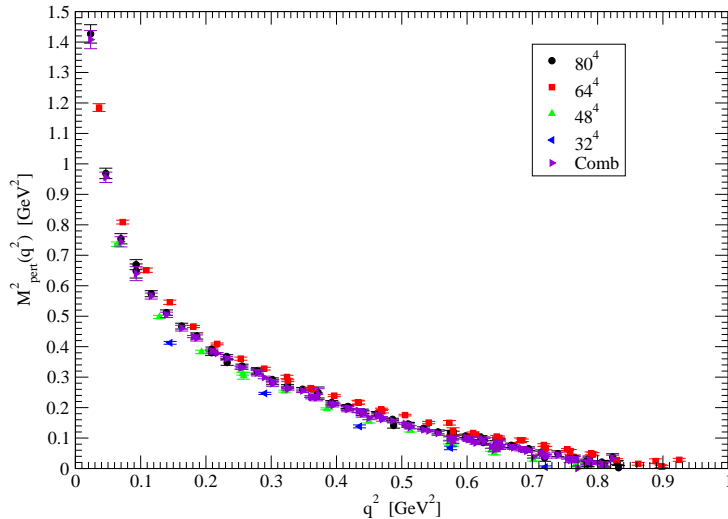


Figure 6. $M_{pert}^2(q^2)$ for the various data sets. Only statistical errors from the propagators are taken into account. Statistical errors were computed assuming gaussian error propagation.

freedom, i.e. for $q_{min} = 3$ GeV, to compute $M^2(q^2)$.

Figure 6 shows $M_{pert}^2(q^2)$ for all data sets. The errors on $M_{pert}^2(q^2)$ include only the contribution from the lattice propagator and were computed assuming gaussian error propagation. $M_{pert}(q^2)$ starts at value ~ 1.2 GeV for $q = 153$ MeV and decreases when q^2 increases. For all the data sets and all fits reported in table 4, $M_{pert}(q^2)$ vanishes for momenta around 1 GeV. For the last point included in figure 6, the error bar is of the same order of magnitude as the central value. For momenta above 1 GeV, not shown in figure 6, $M_{pert}^2(q^2)$ starts to fluctuate and the error bars increase.

The data for the different lattices have differences larger than one standard deviation, which is an indication of finite volume effects. Certainly, the inclusion of the errors due to the parameterization of the gluon dressing function used in the computation of $M_{pert}^2(q^2)$ improve the agreement between the different data sets. Note, however, that the figure 6 shows no clear systematic for the observed differences. Indeed, if the 64^4 data is above the 80^4 data, the 48^4 data is below the largest lattice considered in the present work.

Our interpretation of the results summarized in figure 6 being that the gluon can be viewed as having an effective mass for momenta below 1 GeV. For momenta above 1 GeV, the gluon propagator follows closely the perturbative QCD prediction and becomes a massless boson. This behavior helps explaining why equation (4) could be used to describe the lattice propagator for momenta as low as 1.5 GeV - see the renormalization procedure and results described in table 2 of section 2.

3.2.2. Lattice $M^2(q^2)$ and Dyson-Schwinger Results: As discussed in [2], the nonperturbative solution of the QCD Dyson-Schwinger equations allows for a gluon

L	q_{max} (GeV)	z_0	m_0 (GeV)	Λ (GeV)	r	$\chi^2/d.o.f.$
32	2.46	1.019(64)	0.756(13)	2.13(16)	8(1)	1.58
48	2.14	0.90(16)	0.751(43)	2.47(51)	11(6)	1.90
64	2.53	0.940(68)	0.711(17)	2.37(20)	12(3)	1.88
80	4.13	1.189(20)	0.706(16)	1.842(39)	7.49(59)	1.74
32	2.46	1.019(64)	0.756(13)	2.13(16)	8(1)	1.58
48	2.14	0.90(16)	0.751(43)	2.47(50)	11(6)	1.90
64	2.53	0.940(69)	0.711(17)	2.37(20)	12(3)	1.88
80	4.13	1.189(20)	0.706(16)	1.842(39)	7.49(59)	1.74

Table 5. Fits of the lattice data using equation (15) (upper part of table) and (17) (lower part of table) for mass definition. See text for details.

dynamical generated mass. Such a gluon mass was investigated in detail within the so called decoupling solution of the DSE [9, 10, 11, 12, 13]. Typically, the DSE are solved numerically and the numerical solution is fitted to a given functional form for the full momentum range. By an appropriate choice of the fitting function, one can identify both the running gluon dressing function and mass. Here, we would like to check if the same functional forms are able to described the lattice propagator. Therefore, in this section, we will assume that the gluon propagator is given by the (1), with

$$Z(q^2) = \frac{z_0}{\left[\log \frac{q^2 + r m_0^2}{\Lambda} \right]^\gamma}, \quad (14)$$

where γ is the anomalous gluon dimension, m_0 a mass scale and r a numerical factor.

For the effective gluon mass, we will consider two different functional forms. A more sophisticated expression, which incorporates the perturbative QCD ultraviolet prediction at high momenta [10, 11, 12, 13],

$$M_{soph}^2(q^2) = m^2(q^2, m_0^2) \left[\frac{\log \left(\frac{q^2 + f(q^2, m_0^2)}{\Lambda^2} \right)}{\log \left(\frac{f(0, m_0^2)}{\Lambda^2} \right)} \right]^{-3/5}, \quad (15)$$

with

$$f(x, m_0^2) = \rho_1 m_0^2 + \rho_2 m^2(x, m_0^2) \quad \text{and} \quad m^2(x) = \frac{m_0^4}{x + m_0^2}. \quad (16)$$

In the above expressions $\rho_1 = 1/2$ and $\rho_2 = 5/2$. Besides expression (15), we will also consider the expression

$$M_{simp}^2(q^2) = \frac{m_0^4}{q^2 + m_0^2} \quad (17)$$

for the effective gluon mass also used to described the numerical decoupling solution of the DSE.

For the functional forms (15) and (17), the parameters are computed fitting the lattice data via minimization of the $\chi^2/d.o.f.$ For both expressions, we were not able to fit

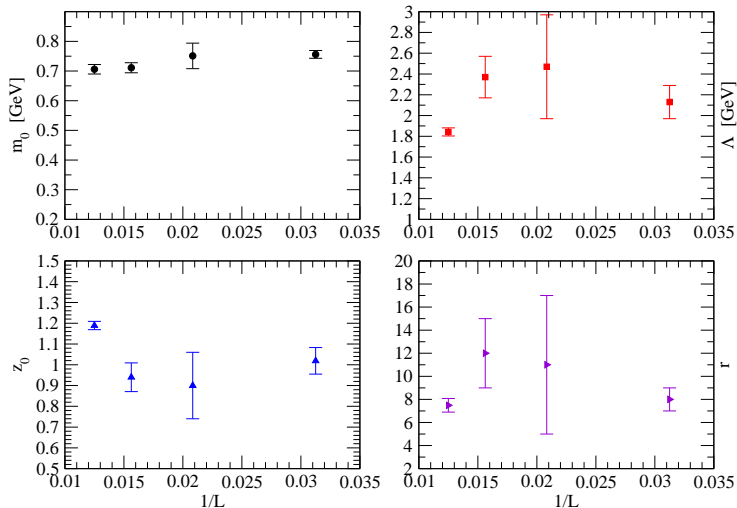


Figure 7. Volume dependence of the parameters defined in (15) and (17).

all momenta range. This can be understood looking at the propagator data in ultraviolet region. Indeed, for large momenta, the statistical errors on the lattice propagator are quite small and the minimization process is constraint mainly by these points. Further, the renormalization process does not eliminate all the artifacts associated the finite lattice spacing. Indeed, a closer look at the propagator show that for $q \sim 5$ GeV and above, the propagators fluctuates slightly. Given the small statistical errors, this makes extremely difficult to fit the data unless the fluctuations are removed as, for example, in [25, 26, 27]. Instead of smoothing our lattice data, we fitted (15) and (17) from $q = 0$ up to q_{max} , where q_{max} was defined as the maximum momentum window where $\chi^2/d.o.f. < 2$.

The fits are reported in table 5. Our first comment being that the fits are not able to distinguish between the two functional forms (15) and (17). The two functional forms describe quite well the lattice propagator in the nonperturbative region, i.e. from zero momentum up to ~ 4.2 GeV. Furthermore, the region which they are able to describe increases with the lattice volume. The exception being the smallest lattice, where the good fit for a relatively large q_{max} is related to the smaller number of *d.o.f.*, which makes the fit easier to perform.

In the infrared region, (15) and (17) reduce to a massive type propagator whose mass is given by the mass parameter m_0 . Looking at the infrared mass computed in section 3.1.1, see table 3, it follows that the hard infrared effective gluon mass is slightly smaller than m_0 . However, m_0 is, within one standard deviation, compatible with the extrapolated infrared mass of 723(11) MeV. Looking at m_0 obtained from the DSE equations, it turns out that their m_0 is slightly smaller than the numbers reported here. For example, in [13] the authors get for $m_0 = 612$ MeV. Note, however, that our definition does not match exactly their definition.

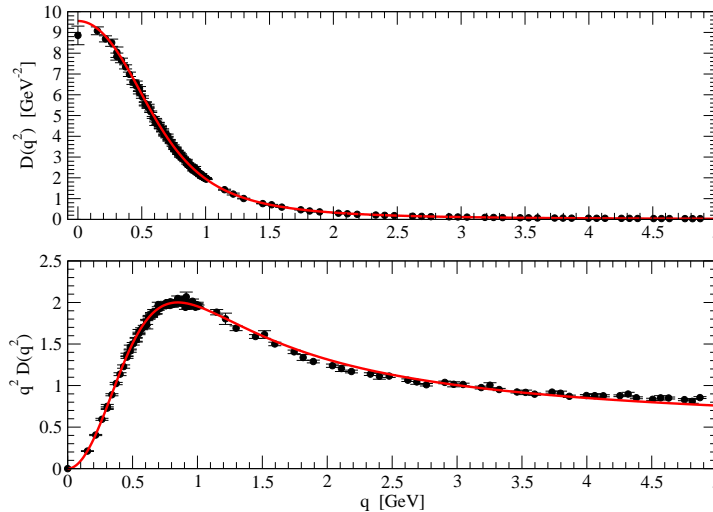


Figure 8. Renormalized gluon propagator and $q^2 D(q^2)$ function from 80^4 lattice data and corresponding using for the mass squared the definition (17).

The volume dependence of the various parameters can be seen in figure 7. m_0 is well described by a linear function of $1/L$, which can be used to extrapolate m_0 to infinite volume. The extrapolation to $V \rightarrow \infty$ gives $m_0 = 671(9)$ MeV, for a $\chi^2/d.o.f. = 0.16$. The extrapolated value is closer to the estimated infrared hard mass measured directly from the lattice data measured in section 3.1.1 and to the DSE estimate for m_0 reported in [13]. For the remaining parameters, it is not clear which functional form should be used to extrapolate to infinite volume and, in the following, we quote the value computed from the largest lattice. Note that all the points for z_0 , Λ and r in figure 7 are compatible within two standard deviations.

From the previous analysis one can conclude that the functional forms used to describe the gluon propagator from the decoupling solution of the Dyson-Schwinger also describe the lattice data. Furthermore, they provide a definition for a dynamical generated gluon mass.

The renormalized gluon propagator and corresponding $q^2 D(q^2)$ function for the 80^4 lattice, together with the fits using (17) to parameterize the running gluon mass, are plotted in figure 8. Figure 9 show the corresponding fitted dressing function and gluon mass.

4. Results and Discussion

In this work we have investigated if the Landau gauge lattice gluon propagator can be described by a massive type propagator. For the gluon mass itself, three different scenarios were considered: i) a constant infrared mass; ii) a constant ultraviolet mass; iii) a running mass in association with a running gluon dressing function. The mass was measured from the momentum space gluon propagator given by equation (1).

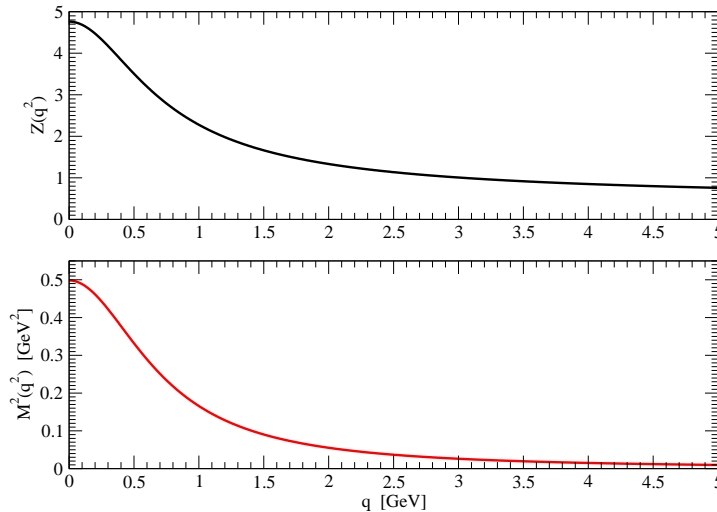


Figure 9. Gluon dressing function and gluon running mass given by (17) from the fits to the largest lattice volume.

The interpretation of the infrared lattice gluon propagator as a massive propagator with constant M and Z was studied in section 3.1.1. Our results show that the lattice data is compatible with such a picture for momenta up to ~ 500 MeV, with an effective gluon mass around 650 - 700 MeV. If the zero momentum gluon propagator is included in the data sets, then the measured $Z = 4.044(78)$ and $M = 648(7)$ MeV. On the other hand, if one removes $D(0)$ from the analysis, $Z = 4.49(10)$ and the effective gluon becomes slightly higher $M = 723(11)$ MeV.

The measured infrared hard mass reproduces the results reported in [5] for SU(3) simulations and is consistent with the quoted infrared mass value estimated for SU(2) in [28], where an M of 0.69(3) GeV or 0.68(4) GeV, depending if one includes or not include $D(0)$ on the analysis, was claimed. Furthermore, the gluon masses claimed above agree well with the estimate of the gluon mass from the gluon condensate $\langle A^2 \rangle$ obtained in [29], where the value 625(33) MeV was obtained, and is well within the interval of values estimated from phenomenology [4].

The interpretation of the lattice gluon propagator as massive type propagator with a constant mass for the ultraviolet region was checked in section 3.1.2. It turns out that the lattice data cannot be fitted consistently by such a propagator. M^2 depends on the fitting range $[q_{min}, q_{max}]$ and, for each q_{max} , M^2 is not constant. This means that, in the ultraviolet, the lattice gluon propagator does not behave as a massive bosonic propagator with a non-vanishing constant mass.

The case of a running gluon mass $M^2(q^2)$ and a running dressing function $Z(q^2)$ was studied in section 3.2. Several definitions for $M^2(q^2)$ together with $Z(q^2)$ were investigated. In general, it turns out that M^2 is a decreasing function of q . Of course, the precise value for $M^2(q^2)$ depends on the chosen definition for $Z(q^2)$ and vice-versa. Here we considered two cases for the dressing function which allow for the computation

of the running mass: (i) a naïve extension of the perturbative dressing function towards the infrared, keeping $Z(q^2)$ always finite; (ii) the functional forms for $M^2(q^2)$ and $Z(q^2)$ used to fit the so-called decoupling type solution of the gluon-ghost Dyson-Schwinger equations.

Our first computation of the gluon running mass considered a parameterization of the running dressing function which extended the perturbative Z towards the infrared region, while keeping $Z(q^2)$ finite for all momenta. The gluon mass defined in this way, $M_{pert}^2(q^2)$ is shown in figure 6. $M(q^2)$ runs from ~ 1.2 GeV for $q = 0$ down to zero for $q \sim 932$ MeV. We would like to call the reader attention, that if instead of using the results reported in table 4 for the larger fitting range, we used the results for the smallest fitting range, the values for $M_{pert}(q^2)$ would be reduced, starting below 1 GeV for the smallest momentum. However, the qualitative behavior will be similar to that observed in figure 6.

After investigating $M_{pert}^2(q^2)$, we have checked the compatibility between the functional forms used to describe the decoupling type solution of the Dyson-Schwinger equations for the gluon propagator and the lattice propagators. These functional forms provide a parametrization of the gluon propagator and a definition for the running gluon mass. Moreover, they take into account the perturbative QCD predictions for the ultraviolet regime. The functional forms are able to describe quite well the lattice data over the entire non-perturbative regime. The lattice data can be fitted by the expressions considered in the present work from $q = 0$ up to q_{max} , with q_{max} increasing with the lattice volume. For our largest volume $q_{max} = 4.13$ GeV. For momenta above ~ 4.13 GeV the remaining lattice spacing effects prevent a fit to the data.

In what concerns the gluon mass, we found that it is well described by

$$M^2(q^2) = \frac{m_0^4}{q^2 + m_0^2}, \quad (18)$$

with $m_0 = 671(9)$ MeV. Our estimation of m_0 agrees well with the estimation performed using the DSE and with is, within errors, compatible with the infrared hard mass when the $D(0)$ was included in the analysis.

From the above results it follows that the interpretation of the gluon propagator as a massive type propagator with a momentum dependent mass and dressing function fits, quite well, the lattice QCD data. The gluon mass is a decreasing function of q^2 and becomes massless in the ultraviolet region. The nature of the gluon mass helps in the understanding of the remarkable mechanism of confinement, where the gluon mass may contribute to a Meissner-type effect in QCD. Moreover, given that one can define an effective gluon mass, it follows that the $\langle A^2 \rangle$ should be taken into account when investigating the non-perturbative dynamics of QCD.

Acknowledgments

The authors acknowledge financial support from F.C.T. under project CERN/FP/83582/2008 and CERN/FP/109327/2009. OO acknowledges FAPES for financial support. The au-

thors thank A. Aguilar for helpful discussions. The authors thank P. J. Silva for the help with the gauge fixing for the 32^4 lattice.

- [1] Faddeev L P and Popov V N 1967 *Phys. Lett B* **25** 29
- [2] Cornwall J H 1982 *Phys. Rev. D* **26** 1453
- [3] Forshaw J R, Papavassiliou J and Parrinello C 1999 *Phys. Rev. D* **59** 074008
- [4] Field J H 2002 *Phys. Rev. D* **66** 013013
- [5] Oliveira O and SILVA P J 2009 Pos (**QCD-TNT09**) 33 (2009) [arXiv:0911.1643].
- [6] Dudal D, Verschelde H, Gracey J A, Lemes V E R, Saranday M S, SObreiro R F and Sorella S P (2004) *JHEP* **401** 44
- [7] Esole M and Freire F (2004) *Phys. Rev. D* **69** 41701
- [8] Dudal D, Oliveira O and Vandersickel N 2010 *Phys. Rev. D* **81** 074505
- [9] Aguilar A C, Natale A A and Rodrigues da Silva P S 2003 *Phys. Rev. Lett.* **90** 152001
- [10] Aguilar A C and Papavassiliou J 2008 *Phys. Rev. D* **77** 125022
- [11] Aguilar A C, Binosi D and Papavassiliou J 2008 *Phys. Rev. D* **78** 025010
- [12] Binosi D and Papavassiliou J 2008 *JHEP* **811** 63
- [13] Aguilar A C and Papavassiliou J 2010 *Phys. Rev. D* **81** 034003 [arXiv:0910.4142]
- [14] Cornwall J M 2009 *Phys. Rev. D* **80** 096001
- [15] Sauli V arXiv:0906.2818 [hep-ph]
- [16] Fischer C S, Maas A and Pawłowski J M 2009 *Ann. Phys.* **324** 2408
- [17] Dudal D, Guimarães M S and Sorella S P, 2011 *Phys. Rev. Lett.* **106**, 062003 [arXiv:1010.3638]
- [18] Dudal D, Gracey J, Sorella S P, Vandersickel N and Verschelde H 2008 *Phys. Rev. D* **78** 065047
- [19] Leinweber D B, Skullerud J I, Williams A G and Parrinello C 1999 *Phys. Rev. D* **60** 094507
- [20] Silva P J and Oliveira O 2004 *Nucl. Phys. B* **690** 177
- [21] Bernard C, Parrinello C and Soni A 1994 *Phys. Rev. D* **49** 1585
- [22] Bali G S and Schilling K 1993 *Phys. Rev. D* **47** 661
- [23] This work was in part based on the MILC collaboration's public lattice gauge theory code: <http://physics.indiana.edu/~sg/milc.html>.
- [24] Bogolubsky I L, Ilgenfritz E-M, Müller-Preussker M and Sternbeck A 2009 *Phys. Lett. B* **676** 69
- [25] Soto F de and Roiesnel C 2007 *JHEP* **709** 7
- [26] Becirevic D, Boucaud Ph, Leroy J P, Micheli J, Pène O, Rodríguez-Quintero J and Roiesnel C 1999 *Phys. Rev. D* **60** 094509 [arXiv:hep-ph/9903364]
- [27] Becirevic D, Boucaud Ph, Leroy J P, Micheli J, Pène O, Rodríguez-Quintero J and C. Roiesnel 2000 *Phys. Rev. D* **61** 114508 [arXiv:hep-ph/9910204]
- [28] Bornyakov V G, Mitrjushkin V K and Müller-Preussker M arXiv:0912.4475
- [29] Arriola E R, Bowman P O and Broniowski W 2004 *Phys. Rev. D* **70** 097505